Research paper

Tilted-hat mushroom billiards: Web-like hierarchical mixed phase space

Diogo Ricardo da Costa [a,b,h,*], Matheus S. Palmero [c], J.A. Méndez-Bermúdez [d,e], Kelly C. Iarosz [c,f], José D. Szezech Jr [g], Antonio M. Batista [c,g]

[a] *Institute of Mathematics and Statistics, University of São Paulo, São Paulo CEP 05508-090, Brazil*
[b] *Postgraduate program in Science/Physics, State University of Ponta Grossa (UEPG), Ponta Grossa 84030-900, PR, Brazil*
[c] *Institute of Physics, University of São Paulo (USP), São Paulo 05508-900, SP, Brazil*
[d] *Departamento de Matemática Aplicada e Estatística, Instituto de Ciências Matemáticas e de Computação, Universidade de São Paulo - Campus de São Carlos, Caixa Postal 668, São Carlos 13560-970, SP, Brazil*
[e] *Instituto de Física, Benemérita Universidad Autónoma de Puebla, Apartado Postal J-48, Puebla 72570, Mexico*
[f] *Graduate Program in Chemical Engineering, Federal Technological University of Paraná, Ponta Grossa, 84016-210, PR, Brazil*
[g] *Departament of Mathematics and Statistics, State University of Ponta Grossa (UEPG), Ponta Grossa 84030-000, PR, Brazil*
[h] *Departamento de Física, Universidade Estadual Paulista (UNESP), Instituto de Geociências e Ciências Exatas, Campus Rio Claro, Av. 24A, 1515, 13506-900 SP, Brazil*

A R T I C L E I N F O

A B S T R A C T

Mushroom billiards are formed, generically, by a semicircular hat attached to a rectangular stem. The dynamics of mushroom billiards shows a continuous transition from integrability to chaos. However, between those limits the phase space is sharply divided in two components corresponding to regular and chaotic orbits, in contrast to most mixed phase space billiards. In this paper we show that tilting the hat of a mushroom billiard produces a highly non-trivial (i.e. non-KAM) mixed phase space. Moreover, for small tilting, this phase space shows a web-like hierarchical structure.

© 2020 Elsevier B.V. All rights reserved.

1. Introduction

Mushroom billiards, also known as Bunimovich mushroom billiards, were introduced by L. A. Bunimovich in the early 2000's [1,2]; since then they have been extensively studied [3–30]. In their most generic version, mushroom billiards are formed by a semicircular hat attached to a rectangular stem. Thus, in one limit they reproduce a half-circle billiard (when the stem has zero hight or zero width) while in the other limit they become a half-stadium billiard (where the width of the stem equals the diameter of the hat). Between those limits their phase space is divided in two well-separated components corresponding to regular and chaotic orbits. Therefore in the transition from integrability to full chaos the relative volume of integrable-to-chaotic phase space can be computed with high accuracy [23].

Mushroom billiards have become paradigmatic models in classical chaos studies, see e.g. [1–4,27], though they do not show the standard Kolmogorov-Arnold-Moser (KAM) scenario. From the classical dynamics point of view, one of the most relevant characteristics of mushroom billiards is the presence of marginally unstable periodic orbits (MUPOs) [3,27] which are the mechanism for the stickiness of chaotic trajectories near the border with the regular phase space component. Even

---

* Corresponding author.
  E-mail address: diogocost2@gmail.com (D.R. da Costa).

if MUPOs present zero measure, they govern the classical dynamics of mushroom billiards leading to distributions with power-law decaying tails of (i) recurrence times, where the decay exponent is two [3,4,8], and (ii) the survival probability in open mushrooms, where the decay exponent is one [25]. Also, quantum or wave versions of mushroom billiards have been implemented (see e.g. [9,11,13,14,17,21,23,24]) where the corresponding eigenvalues and eigenstates have been computed and discussed in terms of quantum chaos concepts. Indeed, the absence of the KAM scenario makes mushroom billiards an ideal model to study integrable-to-chaos wave tunneling [13,14,23]. Beyond that, the study of optical microcavities with the shape of mushroom billiards was carried out in [20,26]. In addition, there are semiclassical [13,20,30] and relativistic quantum chaos [29] studies on mushroom billiards available in the literature. Moreover, the experimentation of mushroom billiards as microwave cavities is reported in Refs. [10,14,17,19,21] where several predictions from quantum chaos studies have been already verified.

Along the years, several deformations have been suggested and applied to the standard (i.e., semicircular hat+rectangular stem) mushroom billiards. Among them, we can mention: triangular stems (see e.g. [1–3,10,15]), elliptical hats [1,6,7], parabolic hats [8], tilted hats [5,18], rounded corners [18], etc. More complex constructions are three-dimensional versions of mushroom billiards [1,25], mushroom "omelets" [1,16], and mushrooms with oscillating boundaries [28]. In this work, we consider mushroom billiards with tilted hats. In particular, we show that tilting the hat of a mushroom billiard destroys the sharp division of the phase space (characteristic of the standard mushroom billiard), producing two seas of chaotic motion separated by a mixed phase space region. Remarkably, the mixed phase space region presents a highly non-trivial, i.e. non-KAM, web-like hierarchical structure whose size and structure depends on the hat tilting. We also show that the web-like structure is supported by hierarchical stability islands produced by particle trajectories located in the mushroom hat, i.e. which do not visit the mushroom stem. Moreover, we provide evidence that the mixed phase space works as a sticky barrier for trajectories moving between the chaotic components of the phase space.

It is fair to add that the deformation we consider here has been already applied to mushroom billiards in Refs. [5,18]. However, the corresponding phase space was not explored in full detail as we do it below.

2. Tilted-hat mushroom billiards

We consider the tilted-hat mushroom billiard of Fig. 1. We set the radius of the outer boundary of the hat of the mushroom billiard to 1, in arbitrary units. So the geometrical parameters characterizing this billiard are: The width of the stem $0 < B < 2$, the height of the stem $0 \leq H < \infty$, and the left and right hat-tilting angles $-\pi/2 \leq \gamma_{l,r} \leq \pi/2$. Notice that γ_l and γ_r are measured clockwise and counterclockwise, respectively, with respect to the horizontal axis. When $\gamma_l = \gamma_r = 0$ the standard mushroom billiard is recovered, see e.g. Fig. 2(a–c); while for $B = 2$ and any $H > 0$ the Bunimovich stadium is obtained [31]. In the later case the hat-tilting angles $\gamma_{l,r}$ can not be specified.

In the next Section, we explore the dynamics of a classical point particle of unit mass bouncing inside tilted-hat mushroom billiards. We choose the initial angle θ_0, see Fig. 1, so that the initial position (X_0, Y_0) of the particle is

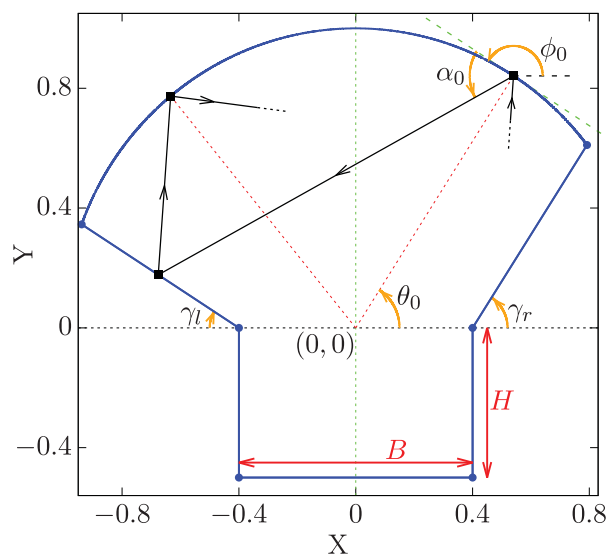$$X_0 = \cos(\theta_0) \quad \text{and} \quad Y_0 = \sin(\theta_0). \tag{1}$$

Fig. 1. (Color online) Sketch of the tilted-hat mushroom billiard. The geometrical parameters characterizing the billiards are: *B*, *H*, γ_l, and γ_r. Here we use $B = 0.8$, $H = 0.5$, $\gamma_l = \pi/2 - 1$, and $\gamma_r = 1$. The radius of the mushroom hat is set to one. We also show a piece of a particle trajectory starting and ending at the outer part of the hat; we choose $\theta_0 = 1$ and $\alpha_0 = \pi/2 - 0.5$.
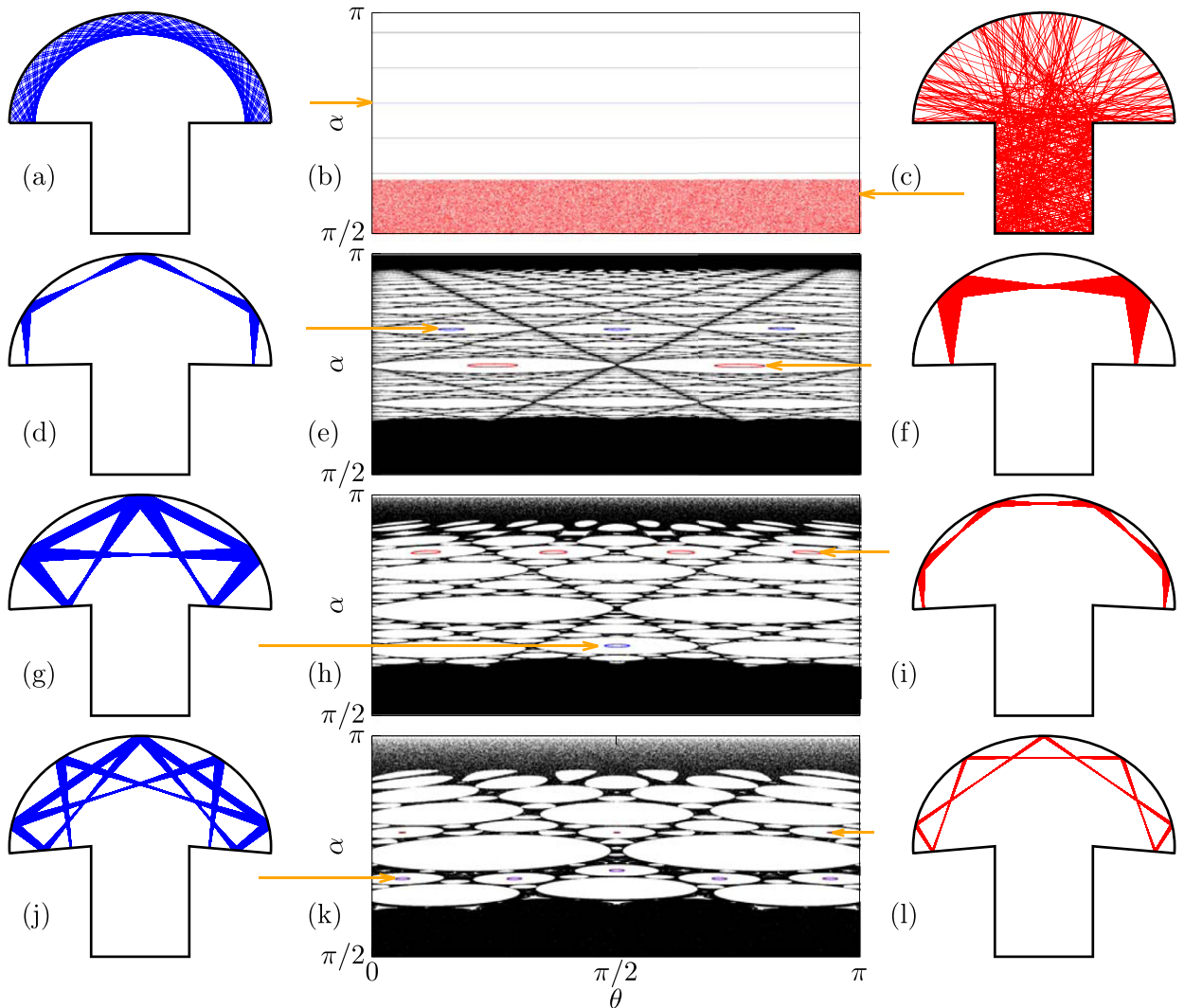
Fig. 2. (Color online) Phase space portraits and selected trajectories for (a–c) the standard mushroom billiard ($\gamma_l = \gamma_r = 0$) and (d–l) symmetric tilted-hat mushroom billiards ($\gamma_l = \gamma_r \neq 0$). We used (d–f) $\gamma_l = \gamma_r = -0.02$, (g-i) $\gamma_l = \gamma_r = -0.06$, and (j-l) $\gamma_l = \gamma_r = -0.1$. $H = 1$ and $B = 0.75$ in all cases. Only half of the phase portraits are shown since the other half, i.e. $0 \leq \alpha \leq \pi/2$, is mirror symmetric. (For interpretation of the references to color in this figure legend, the reader is referred to the web version of this article.)

The range of θ_0 depends on the billiard parameters, for example: If $\gamma_l = \gamma_r = 0$ then $0 \leq \theta_0 \leq \pi$, but if $\gamma_l = \gamma_r = -\pi/2$ and $B = 0$ then $0 \leq \theta_0 \leq 2\pi$. ϕ_0 in Fig. 1 measures the angle between the tangent line to the external hat boundary at (X_0, Y_0) and the horizontal axis, and given by

$$\phi_0 = \arctan\left[\frac{X_0}{-Y_0}\right]. \tag{2}$$

Finally, α_0 is the angle between the tangent line to the external hat boundary at (X_0, Y_0) and the outward particle trajectory (see Fig. 1 for details); $0 \leq \alpha_0 \leq \pi$.

Below we construct phase space portraits by recording the angles (θ, α) along the particle trajectory each time it hits the outer hat boundary.

3. Phase space exploration

Fig. 2 shows phase space portraits and selected trajectories for tilted-hat symmetric mushroom billiards, i.e. when $\gamma_l = \gamma_r$; here we set $H = 1$ and $B = 0.75$ in all cases. We decide to plot only half of the phase portraits since the other half, i.e. $0 \leq \alpha \leq \pi/2$, is mirror symmetric.
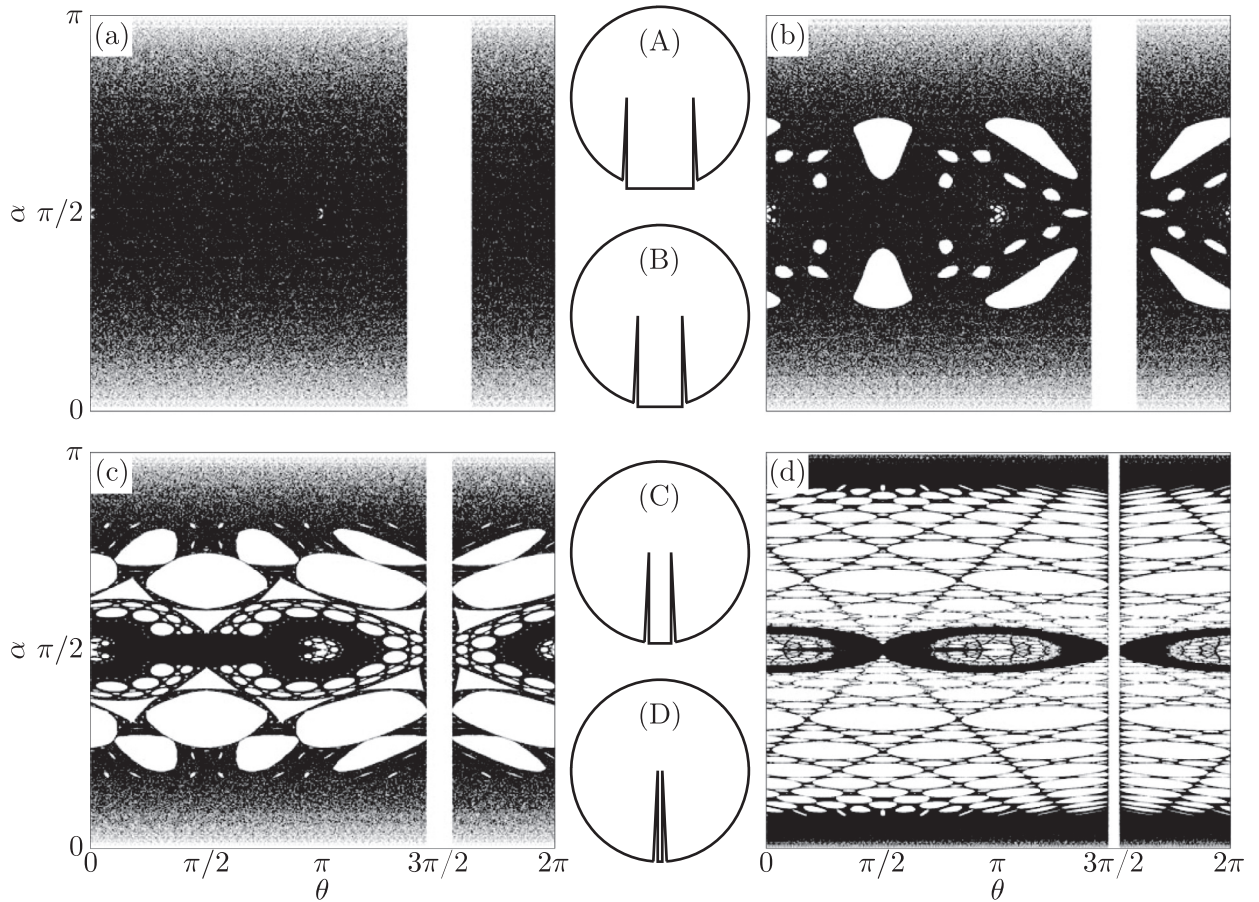
Fig. 3. (Color Online) Phase space portraits for symmetric tilted-hat mushroom billiards with (a) $B = 0.75$, (b) $B = 0.5$, (c) $B = 0.25$, and (d) $B = 0.05$. $H = 1$ and $\gamma_l = \gamma_r = -\pi/2 + 0.05$ in all cases. In (A,B,C,D) the corresponding billiards are shown.

First, as a reference, in Fig. 2(a–c) we present the standard mushroom billiard, $\gamma_l = \gamma_r = 0$. There, it is clear that the phase space is divided in two well-separated components corresponding to regular and chaotic orbits, see Fig. 2(b). We also show examples of regular and chaotic orbits in Fig. 2(a,c), respectively.

Then, Fig. 2(d–l) correspond to symmetric (i.e., $\gamma_l = \gamma_r$) tilted-hat mushroom billiards. We want to note that once $\gamma_l = \gamma_r \neq 0$ the boundary between the chaotic sea (centered at $\alpha = \pi/2$) and the integrable region of the standard mushroom billiard disappears, giving rise to two additional chaotic regions located close to $\alpha = 0, \pi$. Moreover, the phase space region between the chaotic layers becomes mixed and develops sets of periodic and quasi-periodic orbits. In Fig. 2(e,h,k) we show phase space portraits for increasing tilting angles; also, we present examples of typical quasi-periodic orbits [4]. We want to stress that for small tilting angles the periodic and quasi-periodic orbits in between chaotic regions are arranged in a hierarchical-like pattern, see for example the phase space portrait of Fig. 2(e) where $\gamma_l = \gamma_r = -0.02$ is used. Notice that to construct the phase space portrait of Fig. 2(e,h,k) a single trajectory, with initial conditions in the chaotic sea centered at $\alpha = \pi/2$, is used.

In Fig. 2(d–l) we have used relatively small tilting angles compared to Fig. 2(a–c), however by increasing further the tilting we observe the shrinking of the mixed phase space region between chaotic seas. Indeed when $\gamma_l = \gamma_r \rightarrow -\pi/2$ the phase space is mostly ergodic; see for example the phase space portrait of Fig. 3(a) where we used $\gamma_l = \gamma_r = -\pi/2 + 0.05$ keeping the values of H and B of Fig. 2.

Now in Fig. 3 we explore another scenario. There we fix the hight of the stem and the tilting angles to $H = 1$ and $\gamma_l = \gamma_r = -\pi/2 + 0.05$, respectively, and decrease the width of the stem B. From Fig. 3 we observe that decreasing B produces stability (KAM) island supporting periodic and quasi-periodic orbits, so that the almost ergodic phase space of Fig. 3(a) becomes clearly mixed, see Fig. 3(b,c). Thus, for $B \rightarrow 0$, the phase space gets again a hierarchical web-like structure, see Fig. 3(d). The main difference we find between the web-like structure of the phase portraits of Figs. 2(e) and 3(d) is that in the former supports a chaotic sea around $\alpha = \pi/2$ while in the later a region of mixed dynamics is present. As well as in Fig. 2, the phase space portraits of Fig. 3 are constructed by following a single trajectory. The vertical blank region around $\theta = 3\pi/2$, in the phase space portraits of Fig. 3, correspond to particle collisions with the stem boundary that we do not
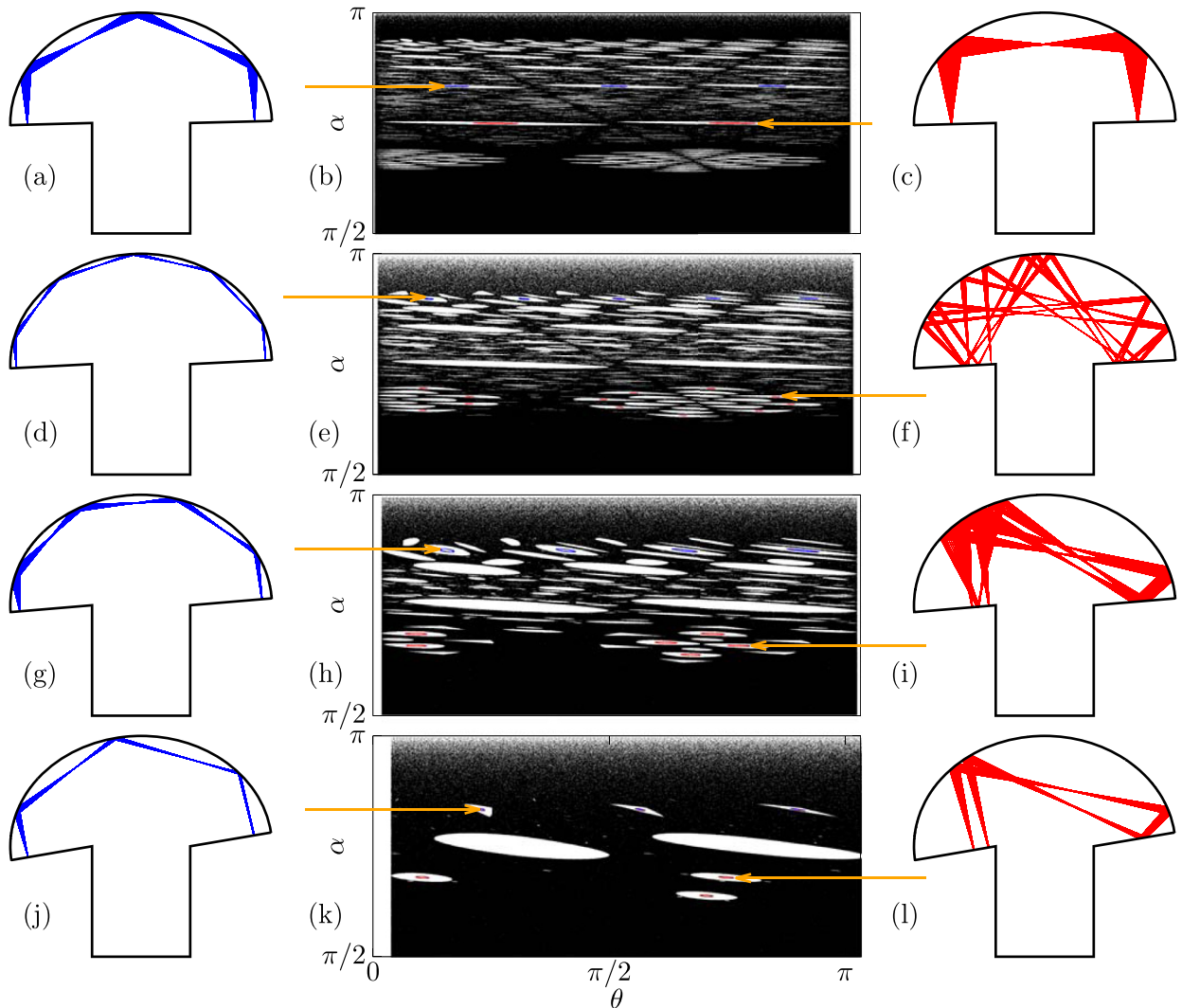
Fig. 4. (Color online) Phase space portraits and selected trajectories for asymmetric tilted-hat mushroom billiards ($\gamma_l = -\gamma_r \neq 0$). We used (a–c) $\gamma_l = -\gamma_r = -0.03$, (d–f) $\gamma_l = -\gamma_r = -0.06$, (g–i) $\gamma_l = -\gamma_r = -0.1$, and (j–l) $\gamma_l = -\gamma_r = -0.2$. $H = 1$ and $B = 0.75$ in all cases. Only half of the phase portraits are shown since the other half, i.e. $0 \leq \alpha \leq \pi/2$, is mirror symmetric.

record; so this region is narrower the smaller the value of B is. We finally note that the case $H = 1$, $B = 0$, and $\gamma_l = \gamma_r = -\pi$ corresponds to a circular barrier billiard (see examples of rectangular barrier billiards in Ref. [32,33]).

In Fig. 4 we consider the asymmetric version of the tilted-hat mushroom billiard. In particular, we choose the case $\gamma_l = -\gamma_r$. We observe a similar panorama as that reported in Fig. 2: Once $\gamma_l = -\gamma_r \neq 0$ the boundary between the chaotic sea and the integrable region of the standard mushroom billiard breaks, giving rise to chaotic regions located close to $\alpha = 0, \pi$; the three chaotic regions are connected through a hierarchical-like mixed phase space region. Also, as expected, in the asymmetric version of the billiard the phase space portraits are non-symmetric. Here, in the prescription $\gamma_l = -\gamma_r$, note that the limit case $H = 1$, $B = 0$, and $\gamma_l = -\gamma_r = -\pi$ corresponds to an integrable half-circular billiard.

Given that the phase space portraits in Figs. 2(e,h,k), 3(a-d), and 4(b,e,h,k) are constructed from the iteration of a single trajectory, it is expected that for a particle moving from the chaotic region around $\alpha = \pi/2$ to the chaotic regions close to $\alpha = 0, \pi$ (and vice-versa) the mixed phase space region in between can serve as a sticky region [3] that should slow down particle diffusion.

To verify this in a graphical way we choose the phase portrait of Fig. 5(a) having parameters $H = 0.005$, $B = 0.2$, and $\gamma_l = \gamma_r = -\pi/2 + 0.001$ (note that we are using a very short and narrow stem, while the mushroom hat is almost a complete circle; as the mushrooms of Fig. 3). Indeed to construct this phase space portrait we used a single trajectory, with an initial condition in the upper chaotic region ($\theta_0 = 2\pi - 0.1$ and $\alpha_0 = 3$), hitting 1.1×10^6 times the outer boundary of the mushroom billiard hat. We emphasize that such long trajectories are needed in order to allow the particle to explore
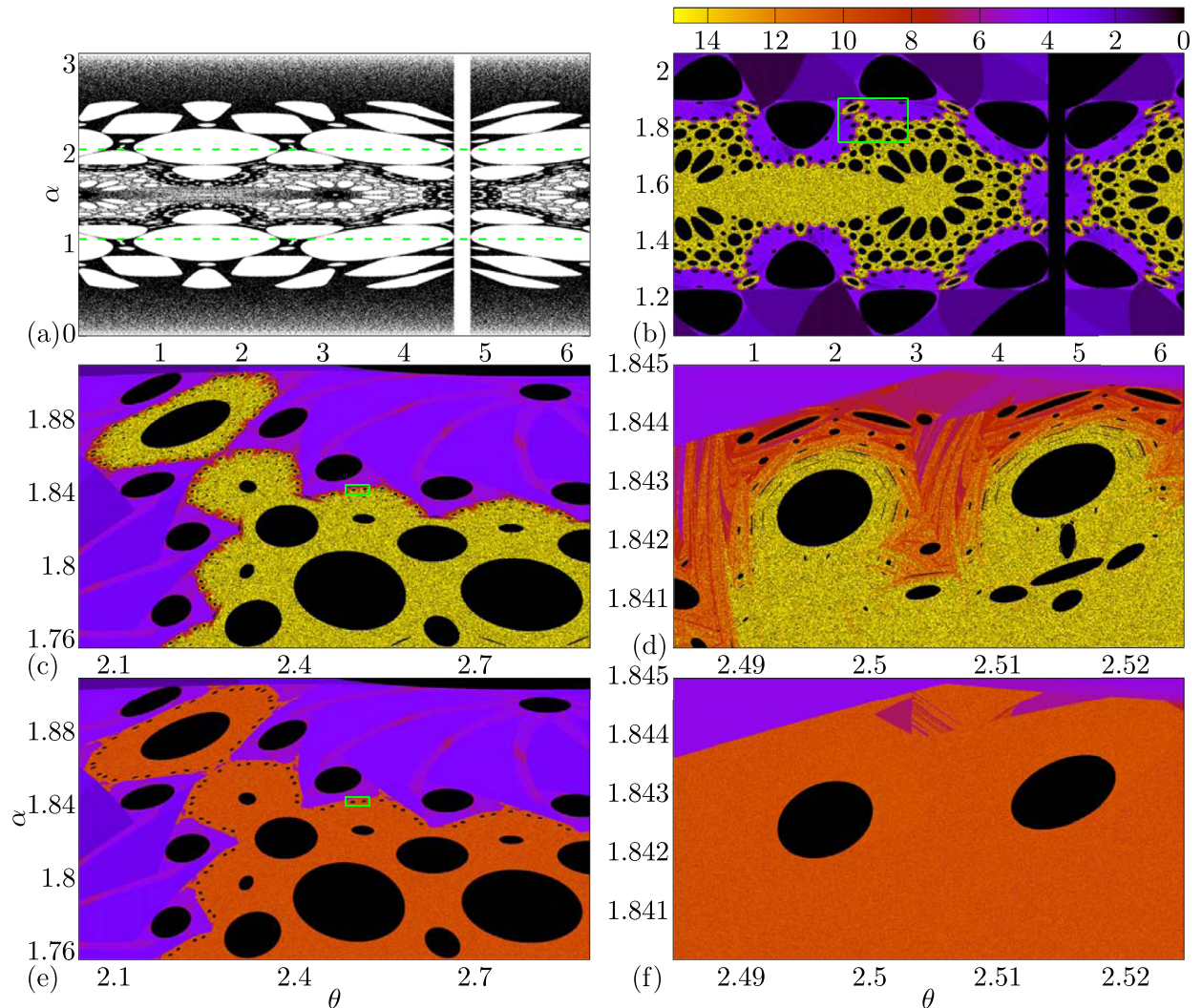
Fig. 5. (Color online) (a) Phase space portrait for the symmetric tilted-hat mushroom billiard with $H = 0.005$, $B = 0.2$, and $\gamma_l = \gamma_r = -\pi/2 + 0.001$. The green dashed lines at $\alpha = \pi/2 \pm 0.5$ indicate escaping thresholds. (b) Stickiness colormap for a grid of 1000×1000 initial conditions (θ_0, α_0) in the phase space interval $\pi/2 - 0.5 < \alpha < \pi/2 + 0.5$. Colors label the number (in log scale) of particle collisions with the outer boundary of the mushroom billiard hat until the particle approaches the escaping thresholds. (c) and (d) are enlargements of the green rectangles in panels (b) and (c), respectively. In (d,e) stickiness colormaps in the same phase space region of panels (c,d) are shown but for a mushroom billiard with $H = 1$. (For interpretation of the references to color in this figure legend, the reader is referred to the web version of this article.)

the mixed phase space region. So, we place a grid of 1000×1000 initial conditions (θ_0, α_0) in the phase space interval $\pi/2 - 0.5 < \alpha < \pi/2 + 0.5$, delimited by the green dashed horizontal lines in Fig. 5(a). Then, we count the number of particle collisions with the outer boundary of the mushroom billiard hat until the particle escapes this phase space region; i.e. until the particle acquires a value of α smaller than $\pi/2 - 0.5$ or larger than $\pi/2 + 0.5$. The result is shown in Fig. 5(b) where the colors indicate the magnitude of the natural logarithm of the number of iterations until the particle escapes. The logarithm function is used to suppress phase space regions with huge counts. From Fig. 5(b) we can clearly see two well defined main phase space regions: One in purple and the other in yellow. These regions are characterized by small and huge stickiness, respectively; that is, a trajectory with initial conditions in the yellow phase space region (near $\alpha = \pi/2$) will take a huge time to leave this region and eventually escape. Black areas in this figure represent periodic or quasi-periodic conditions; i.e. particles with initial conditions there cannot escape. In Fig. 5(c) and (d) we show enlargements of the green rectangles in Fig. 5(b) and (c), respectively, so we can see further details of the escape colormap as well as of the stability island structure of the mixed phase space.

As additional information in Fig. 5(e) and (f) we present colormaps in the interval of phase space than Fig. 5(c) and (d), respectively, where we have increased the hight of the stem to $H = 1$. Notice here that yellow phase space regions are turned into the orange so that the stickiness has been considerably reduced as well as the presence of stability islands. Thus, the
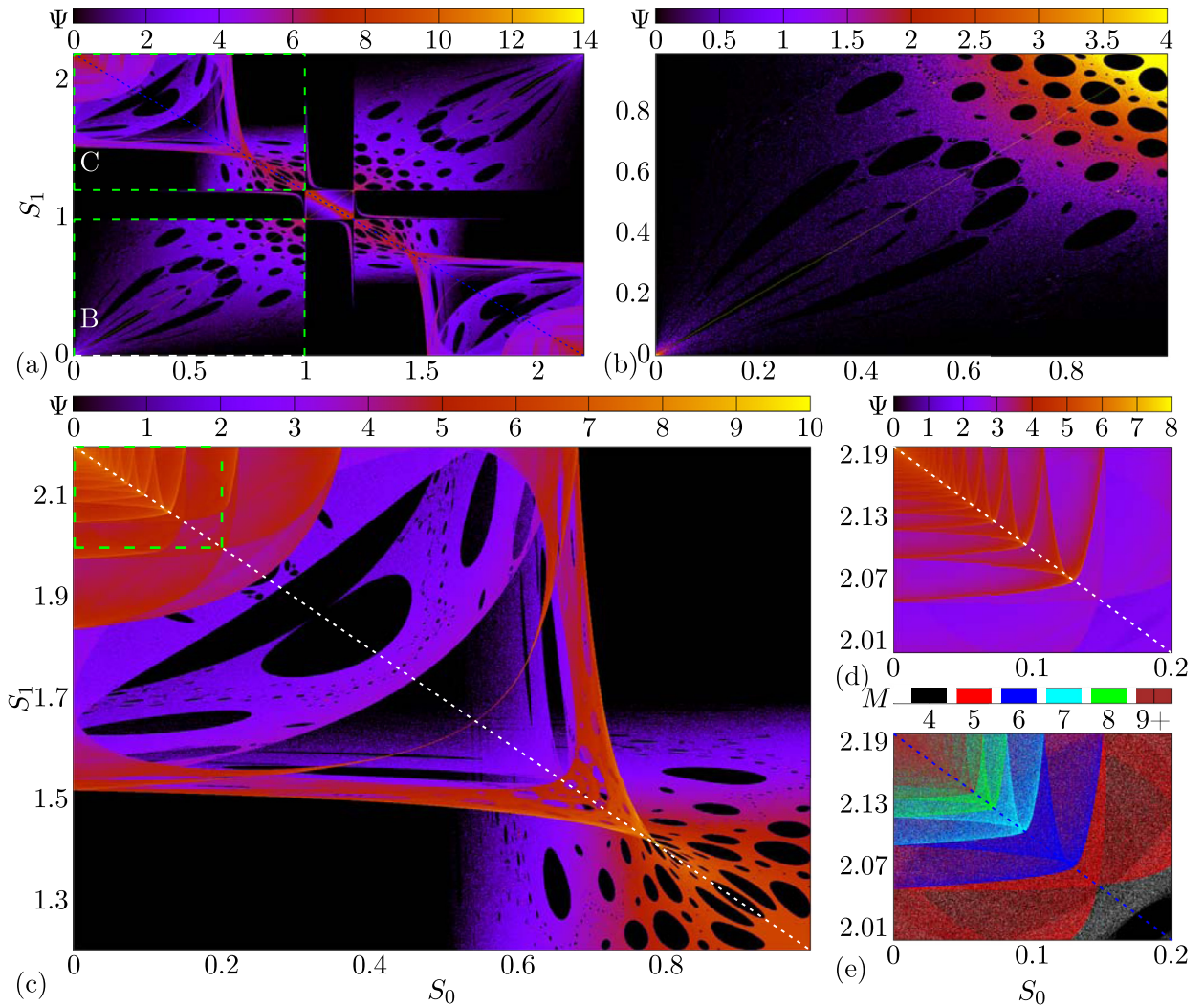
Fig. 6. (Color online) Density plots of Ψ as defined in Eq. (3) for the symmetric tilted-hat mushroom billiard with $H = 0.005$, $B = 0.2$ and $\gamma_l = \gamma_r = -\pi/2 + 0.001$. (b) and (c) are the enlargements of the regions of panel (a) labeled as B and C, respectively. (d) is the enlargement of the green dashed rectangle in panel (c). (e) Shows the counting of successive particle reflections with the hat of the billiard. (For interpretation of the references to color in this figure legend, the reader is referred to the web version of this article.)

height of the stem has an important role in the phase space fine structure a stickiness that will be properly characterized in a future study.

In an attempt to discover structures not exposed in the phase space portraits reported above, we construct density plots for the mapping $S_1 = \mathcal{M} S_0$, where $S_{0,1}$ is the arc length (measured counterclockwise relative to the left corner of the mushroom hat) of a given n-th hit of the particle trajectory with the outer boundary of the mushroom hat. See for example Fig. 6.

Specifically, in order to construct Fig. 6 we follow a single particle (with initial angles $\theta_0 = 0.5$ and $\alpha_0 = 2.5$) until hitting 10^9 times the outer boundary of the mushroom hat. Each time the particle hits one of the straight-line segments of the mushroom hat we record the previous arc length position S_n that we call S_0, we then call S_1 the corresponding S_n of the next hit of the particle with a straight line segment and so on. We count the number of times Σ the trajectory visits the boxes in a grid of 1000×1000 equally spaced intervals in the $S_1 S_0$ plane along the orbit. In particular we define the quantity Ψ as the natural logarithm of Σ:

$$\Psi = \ln(\Sigma). \tag{3}$$

Here, the logarithm function is used to suppress regions with huge counts. Then, in Fig. 6(a) we present the density plot of Ψ for the symmetric tilted-hat mushroom billiard with $H = 0.005$, $B = 0.2$ and $\gamma_l = \gamma_r = -\pi/2 + 0.001$; i.e., the same mushroom parameters used in Fig. 5. Clearly, Fig. 6(a) shows highly nontrivial structures enlarged in panels (b–d). In particular, black islands correspond to the phase space periodic and quasi-periodic islands.

Moreover, in Fig. 6 we detect self-similar structures at opposite corners of the main diagonal of the $S_0 S_1$ plane; see the dashed green rectangle in Fig. 6(c) which is magnified in Fig. 6(d). Similar structures were recently reported in Ref. [34] for a two-dimensional map describing the dynamics of classical particles in a time-dependent potential well. There, the self-similar structures were produced by continuous particle reflections within the time-dependent well. However, self-similar structures can also be produced by whispering gallery orbits in billiards with concave walls as shown in Mendez-Bermudez et al. [35], Felix and Pagneux [36], which is the origin of the structures we observe here. Indeed, to verify this, we have recorded the number of times M the particle hits the outer boundary of the mushroom hat in between consecutive hits with the straight-line segments of the mushroom hat. In Fig. 6(e) we report M in the same part of the $S_0 S_1$ plane than Fig. 6(d). In fact, Fig. 6(e) shows that the outer swallow-like layer forming the self-similar structure in Fig. 6(d), with edge at $S_0 \approx 0.15$, is produced by trajectories characterized by $M = 5$. The next swallow-like layer with edge at $S_0 \approx 0.125$ is formed by trajectories with $M = 7$, third next corresponds to trajectories having $M = 8$, and so on. Thus, in Fig. 6(d) the accumulation point at $S_0 \rightarrow 0$, and $\max(S_1)$, corresponds to $M \rightarrow \infty$ and is approached when orbits approach the corner of the mushroom hat; i.e., a billiard boundary point with undefined derivative, known in the literature as a cusp [37].

4. Conclusions

In this paper we study tilted-hat mushroom billiards and present detailed portraits of the corresponding phase space. We emphasize the dynamical richness of this billiard model since by the proper parameter setting it reproduces well known billiards: the ergodic Bunimovich stadium, the integrable semicircular billiard, the standard mushroom billiard (semicircular hat+rectangular stem) which presents a sharply divided phase space, a quasi-integrable circular barrier-billiard, and, consequently, many other billiards in between.

In particular, we show that small hat tilting induces a highly non-trivial (i.e. non-KAM) hierarchical mixed phase space, presenting a web-like hierarchical structure, which separates two regions of chaotic motion; thus, destroying the sharply divided phase space proper of the standard mushroom billiard. As clearly shown in Fig. 2, the mixed phase space is supported by a hierarchical set of stable islands produced by particle trajectories located in the mushroom hat. Moreover, in the large-period limit, those trajectories become whispering gallery orbits that in turn produce fractal-like patters in orbit-density plots, as presented in Fig. 6. We want to stress that the web-like mixed phase space we report here works as a sticky barrier for trajectories moving between the chaotic components of the phase space. This may strongly affect the dynamical properties (i.e. diffusion and escape) of trajectories in tilted-hat mushroom billiards.

In future works, we plan to develop a theoretical approach to our results.

Declaration of Competing Interest

The authors declare that they have no known competing financial interests or personal relationships that could have appeared to influence the work reported in this paper.

Supplementary material

Supplementary material associated with this article can be found, in the online version, at doi:10.1016/j.cnsns.2020. 105440.

References

[1] Bunimovich LA. Mushrooms and other billiards with divided phase space. Chaos 2001;11:802–8.
[2] Bunimovich L. Kinematics, equilibrium, and shape in Hamiltonian systems: The "LAB" effect. Chaos 2003;13:903–12.
[3] Altmann EG, Motter AE, Kantz H. Stickiness in mushroom billiards. Chaos 2005;15:033105.
[4] Altmann EG, Motter AE, Kantz H. Stickiness in Hamiltonian systems: From sharply divided to hierarchical phase space. Phys Rev E 2006;73:026207.
[5] Dietz B, Friedrich T, Miski-Oglu M, Richter A, Seligman TH, Zapfe K. Nonperiodic echoes from mushroom billiard hats. Phys Rev E 2006;74:056207.
[6] Lansel S, Porter MA, Bunimovich LA. One-particle and few-particle billiards. Chaos 2006;16:013129.
[7] Porter MA, Lansel S. Mushroom billiards. Notices AMS 2006;53:334–7.
[8] Tanaka H, Shudo A. Recurrence time distribution in mushroom billiards with parabolic hat. Phys Rev E 2006;74:036211.
[9] Barnett AH, Betcke T. Quantum mushroom billiards. Chaos 2007;17:043125.
[10] Dietz B, Friedrich T, Miski-Oglu M, Richter A, Schafer F. Spectral properties of Bunimovich mushroom billiards. Phys Rev E 2007;75:035203.
[11] deMenezes DD, eSilva MJ, deAguiar FM. Numerical experiments on quantum chaotic billiards. Chaos 2007;17:023116.
[12] Miyaguchi T. Escape time statistics for mushroom billiards. Phys Rev E 2007;75:066215.

[13] Vidmar G, Stöckmann H-J, Robnik M, Kuhl U, Höhmann R, Grossmann S. Beyond the Berry-Robnik regime: A random matrix study of tunneling effects. J Phys A: Math Theor 2007;40:13883–905.
[14] Bäcker A, Ketzmerick R, Löck S, Robnik M, Vidmar G, Höhmann R, Kuhl U, Stöckmann HJ. Dynamical tunneling in mushroom billiards. Phys Rev Lett 2008;100:174103.
[15] Bunimovich LA. Chaotic and nonchaotic mushrooms. Discrete Contin Dyn Syst 2008;22:63–74.
[16] Bunimovich LA. Relative volume of Kolmogorov-Arnold-Moser tori and uniform distribution, stickiness and nonstickiness in Hamiltonian systems. Nonlinearity 2008;21:T13–17.
[17] Abul-Magd AY, Dietz B, Friedrich T, Richter A. Spectral fluctuations of billiards with mixed dynamics: From time series to superstatistics. Phys Rev E 2008;77:046202.
[18] Zapfe K, Leyvraz F, Seligman TH. About imperfect mushroom billiards, arXiv:0805.3727 2008.
[19] Bäcker A, Dietz B, Friedrich T, Miski-Oglu M, Richter A, Schafer F, Tomsovic S. Friedel oscillations in microwave billiards. Phys Rev E 2009;80:066210.
[20] Andreasen J, Cao H, Wiersig J, Motter AE. Marginally unstable periodic orbits in semiclassical mushroom billiards. Phys Rev Lett 2009;103:154101.
[21] Dietz B, Friedrich T, Miski-Oglu M, Richter A, Schafer F, Seligmann TH. Nonperiodic echoes from quantum mushroom-billiard hats. Phys Rev E 2009;80:036212.
[22] Plakhov AY. Scattering in billiards and problems of Newtonian aerodynamics. Russian Math Surveys 2009;64:873–938.
[23] Batistic B, Robnik M. Semiempirical theory of level spacing distribution beyond the Berry-Robnik regime: modeling the localization and the tunneling effects. J Phys A: Math Theor 2010;43:215101.
[24] Bäcker A, Ketzmerick R, Löck S, Schanz H. Partial Weyl law for billiards. Europhys Lett 2011;94:30004.
[25] Dettmann CP, Georgiou O. Open mushrooms: stickiness revisited. J Phys A: Math Theor 2011;44:195102.
[26] Tsugawa S, Satoru Y. Stagnant motion in chaotic region of mushroom billiard system with dielectric medium. J Phys Soc Japan 2012;81:064004.
[27] Bunimovich LA. Fine structure of sticky sets in mushroom billiards. J Stat Phys 2014;154:421–31.
[28] Gelfreich V, Rom-Kedar V, Turaev D. Oscillating mushrooms: adiabatic theory for a non-ergodic system. J Phys A: Math Theor 2014;47:395101.
[29] Huang L, Xu HY, Grebogi C, Lai YC. Relativistic quantum chaos. Phys Rep 2018;753:1–128.
[30] Gomes SP. Percival's conjecture for the Bunimovich mushroom billiard. Nonlinearity 2018;31:4108–36.
[31] Bunimovich LA. On the ergodic properties of nowhere dispersing billiards,. Commun Math Phys 1979;65:295.
[32] Bogomolny E, Dietz B, Friedrich T, Miski-Oglu M, Richter A, Schäfer F, Schmit C. First experimental observation of superscars in a pseudointegrable barrier billiard. Phys Rev Lett 2006;97:254102.
[33] Aberg S, Guhr T, Miski-Oglu M, Richter A. Superscars in billiards: A model for doorway states in quantum spectra. Phys Rev Lett 2008;100:204101.
[34] daCosta DR, Mendez-Bermudez JA, Leonel ED. Scaling and self-similarity for the dynamics of a particle confined to an asymmetric time-dependent potential well. Phys Rev E 2019;99:012202.
[35] Mendez-Bermudez JA, Luna-Acosta GA, Seba P, Pichugin KN. Understanding quantum scattering properties in terms of purely classical dynamics: Two-dimensional open chaotic billiards. Phys Rev E 2002;66:046207.
[36] Felix S, Pagneux V. Ray-wave correspondence in bent waveguides. Wave Motion 2005;41:339.
[37] Chernov N, Markarian R. Dispersing billiards with cusps: Slow decay of correlations. Commun Math Phys 2007;270:727.